pubs.acs.org/JACS

Article

Organ/Cell-Selective Intracellular Delivery of Biologics via *N*-Acetylated Galactosamine-Functionalized Polydisulfide Conjugates

Jianhua Lu, Yuanhao Dai, Yahui He, Ting Zhang, Jing Zhang, Xiangmei Chen, Changtao Jiang, and Hua Lu*

Cite This: *J. Am. Chem. Soc.* 2024, 146, 3974−3983

Read Online

ACCESS | Metrics & More | Article Recommendations | Supporting Information

ABSTRACT: Biologics, including proteins and antisense oligonucleotides (ASOs), face significant challenges when it comes to achieving intracellular delivery within specific organs or cells through systemic administrations. In this study, we present a novel approach for delivering proteins and ASOs to liver cells, both *in vitro* and *in vivo*, using conjugates that tether *N*-acetylated galactosamine (GalNAc)-functionalized, cell-penetrating polydisulfides (PDSs). The method involves the thiol-bearing cargo-mediated ring-opening polymerization of GalNAc-functionalized lipoamide monomers through the so-called aggregation-induced polymerization, leading to the formation of site-specific protein/ASO-PDS conjugates with narrow dispersity. The hepatocyte-selective intracellular delivery of the conjugates arises from a combination of factors, including first GalNAc binding with ASGPR receptors on liver cells, leading to cell immobilization, and the subsequent thiol−disulfide exchange occurring on the cell surface, promoting internalization. Our findings emphasize the critical role of the close proximity of the PDS backbone to the cell surface, as it governs the success of thiol−disulfide exchange and, consequently, cell penetration. These conjugates hold tremendous potential in overcoming the various biological barriers encountered during systemic and cell-specific delivery of biomacromolecular cargos, opening up new avenues for the diagnosis and treatment of a range of liver-targeting diseases.

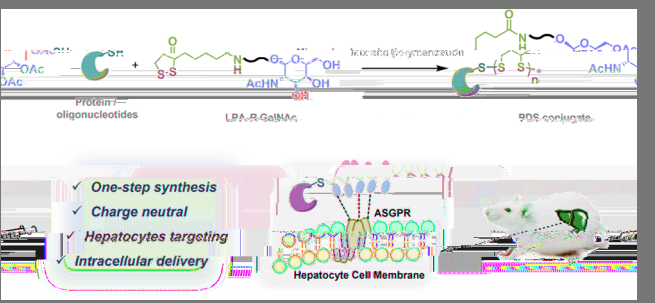

INTRODUCTION

Biomacromolecules, encompassing a wide spectrum of therapeutics such as antibodies, recombinant proteins, peptides, mRNA, siRNA, and antisense oligonucleotides (ASOs), have emerged as a highly useful and rapidly advancing category of medical treatments for their exceptional potency and specificity.[1−7] However, the challenge of achieving selective intracellular delivery to specific organs or cells through systemic administration remains a substantial hurdle in clinical applications.[8−11] This challenge stems from both the inherent vulnerability and substantial size of biomacromolecules as well as the complex and sometimes conflicting requirements for overcoming various biological barriers at different scales. Targeting specific cells or organs has been achieved through the development of ligands, such as antibodies, peptides, aptamers, and small molecules, or through *in vivo* screening systems like CELEX, ATTACK, and SORT.[12−15] Notably, liver-specific targeting has been accomplished using trivalent *N*-acetylated galactosamine (GalNAc) ligands, leading to the approval of several siRNA and ASO drugs on the market.[16−21] However, cargo delivered via the asialoglycoprotein receptor (ASGPR)-mediated internalization pathway often becomes trapped within endosome/lysosome compartments, necessitating high drug doses in clinical use. To address these challenges, intracellular delivery systems for biomacromolecules have been developed in recent years, including lipid nanoparticles, polymers, and organic−inorganic hybrid systems such as metal−organic frameworks.[22−33] Still, dose-limiting cationic (ionizable) components are often required to facilitate endosomal escape, irrespective of the distinct physicochemical properties of protein and nucleic acid cargos, potentially leading to systemic cytotoxicity.[34] Additionally, the efficiency of intracellular delivery can be compromised by the ineffective release of the cargo from the carrier system.[35−37] To this end, it is important to develop a simple, charge neutral, yet highly effective delivery system capable of addressing multiple challenges, including targeting,

Received: October 25, 2023
Revised: January 15, 2024
Accepted: January 18, 2024
Published: February 1, 2024

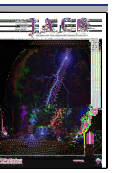

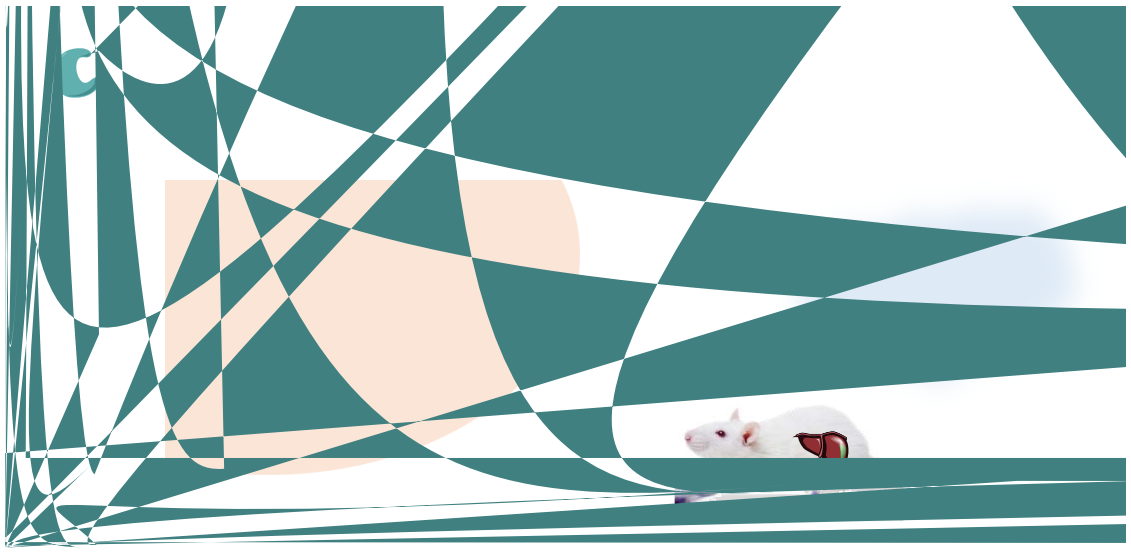

Figure 1. Schematic illustration of the grafting-from synthesis and targeted intracellular delivery of protein/oligonucleotide−PDS conjugates into liver cells.

cell penetration, and controlled intracellular release in a spatially and temporally controlled manner.[38−55]

Here, we report a streamline strategy employing GalNAc-functionalized polydisulfide (PDS) for the delivery of biologics, proteins, and ASOs, for example, into liver cells. The system is ultimately simple, requiring only a single-step, room-temperature mixing of thiol-functionalized protein/oligonucleotides (ONDs) with GalNAc-functionalized 1,2-dithiolane monomers to create the corresponding PDS conjugates (Figure 1). The GalNAc-functionalized PDS possesses a neutral charge, facilitates liver cell targeting through GalNAc-ASGPR recognition, and achieves selective internalization via successive PDS-mediated membrane penetration (Figure 1). Moreover, the biomacromolecular cargo can be tracelessly released through PDS degradation triggered by high intracellular glutathione (GSH) concentrations (Figure 1).

RESULTS AND DISCUSSION

Previously, multivalent GalNAc-functionalized polymers and nanoparticles have been developed to encapsulate cargos via various physical interactions.[56−58] Nonetheless, the backbone of these polymers commonly lacked the ability to cross the cell membrane without cations and biodegradability to release cargos intracellularly. For this, we aimed to covalently conjugate GalNAc-functionalized PDS to protein or OND. We envisaged that the covalent conjugation of PDS could avoid premature release *in vivo* and the unique cell-penetrating capability of PDS could facilitate liver cell internalization additional to the ASGPR-mediated endocytosis.[59−71] To ensure satisfactory liver cell targeting, we designed and screened a series of GalNAc-functionalized lipoamide monomers with linkers of different lengths and hydrophobicities (Figure 2A). The monomers were successfully obtained via the synthetic route shown in Figure S1, with the yield above 80% for each step. The molecular identity and purity of the monomers were confirmed by ^{1}H and ^{13}C NMR spectroscopy, and mass spectrometry (MS), which were compiled in Figures 2C and S2−S14. Normally, the bulky glycol side chain and the low ring strain of 1,2-dithiolanes hamper the polymerizability of these monomers. To circumvent this synthetic challenge, we sought to test the recently reported aggregation-induced polymerization (AIP) effect, namely, the aggregation of amphiphilic monomers in aqueous solutions to boost the local monomer concentration and facilitate ROP at concentrations significantly under $[M]_{eq}$, the equilibrium monomer concentration.[72] Indeed, dynamic light scattering (DLS) indicated that the GalNAc-bearing lipoamide monomers formed aggregates in water at roughly 50 mM or higher (Figure S15). To test the polymerizability of these monomers, an enhanced green fluorescent protein mutant containing a reactive cysteine (EGFP-SH) was used as a model initiator (Figure 2B). Among the tested monomers, LPA-EG2GalNAc and LPA-EG3GalNAc had excellent aqueous solubility and were found to polymerize at an initial monomer concentration ($[M]_0$) as low as 100 mM thanks to the AIP effect (Figure 2C). LPA-C2GalNAc and LPA-C3GalNAc, less soluble than the former two, were polymerized at a $[M]_0$ of 200 mM in aqueous solutions containing 20% DMSO. As shown in the nonreducing sodium dodecyl sulfate-polyacrylamide gel electrophoresis (SDS-PAGE), all conjugates were narrowly dispersed with an average apparent molecular weight (MW) of ∼ 45 kDa (Figure 2D). Further analysis of EGFP-*p*(C2GalNAc), the conjugate composed of EGFP and PDS of LPA-C2GalNAc, via SEC (SI) revealed a sharp peak corresponding to an apparent MW of 44 kDa and a dispersity of 1.02 (Figure 2E), which agreed well with the SDS-PAGE result (Figure 2D). The MW and degree of polymerization (DP) of *p*(C2GalNAc) in this sample were thus estimated to be 16 and 35 kDa, respectively. Few free EGFP-SH was left after the polymerization, highlighting the excellent initiation efficiency of this grafting-from strategy. Treating EGFP-*p*(C2GalNAc) with glutathione or other reducing reagents under physiology-relevant conditions fully recovered native EGFP-SH, implying potential ability of traceless cargo release from the conjugate in an intracellular environment (Figure S16).

Next, by measuring the fluorescence of EGFP using flow cytometry, we investigated the hepatocyte-selective delivery of EGFP-*p*(C2GalNAc), a conjugate composed of EGFP and PDS of polymer of LPA-C2GalNAc. HepG2 and HeLa, two human cancer cell lines with high and low expression of

https://doi.org/10.1021/jacs.3c11914
J. Am. Chem. Soc. 2024, 146, 3974−3983

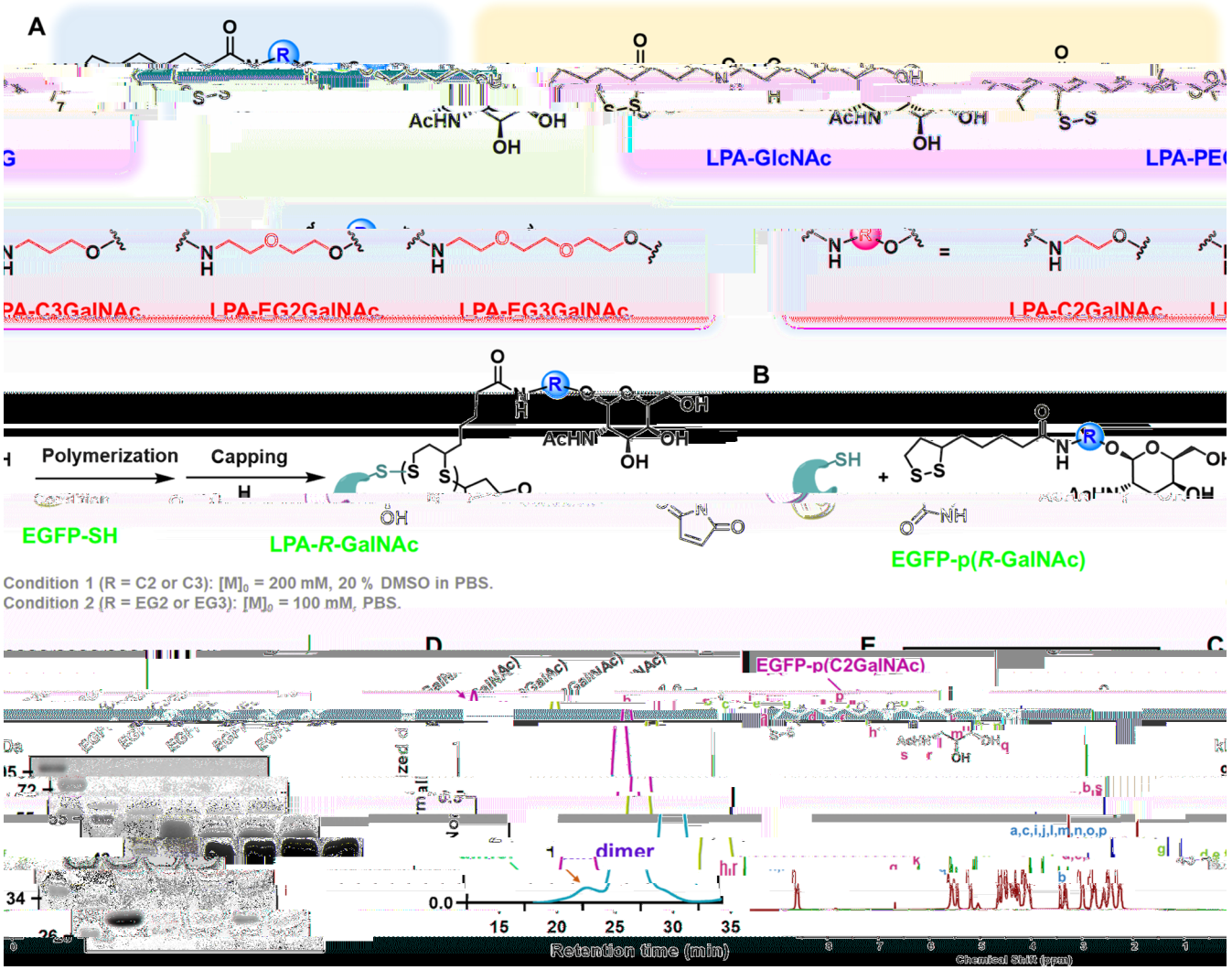

Figure 2. (A) Structures and nomenclature of the GalNAc-functionalized lipoamide monomers (LPA-*R*-GalNAc) used in this study. (B) Synthetic scheme of the EGFP-SH-initiated polymerization of LPA-*R*-GalNAc monomers. (C) ^{1}H NMR spectrum of LPA-C2GalNAc (400 MHz, DMSO-d_6). (D) Nonreducing SDS-PAGE of different EGFP-*p*(*R*-GalNAc) conjugates. All polymerizations were conducted at a $[M]_0/[\text{protein}]$ ratio of 1500/1 and quenched at 4 h with maleimide; $[M]_0$ = 100 or 200 mM. (E) SEC trace of EGFP-*p*(C2GalNAc) analyzed by FPLC equipped with a superdex 200 SEC column, a miniDAWN TREOS laser light scattering detector, and an Optilab T-rEX refractive index detector. The d*n*/d*c* of the conjugate was calculated as 0.185 mL/g. The small shoulder peak denoted by the red arrow is the dimer of the remaining EGFP-SH.

ASGPR, were employed as positive and negative cell line, respectively. To verify the GalNAc-ASGPR-dependent delivery, we also produced two control EGFP-PDS conjugates bearing a *N*-acetylated glucosamine and PEG side chain, namely, EGFP-*p*(GlcNAc) and EGFP-*p*(LPA-PEG), respectively. The three conjugates were made of similar size with a PDS degree of polymerization (DP) of ∼100 (Figure S17). EGFP-*p*(C2GalNAc) showed low uptake by HeLa cells but high HepG2 uptake to a level comparable to the positive control, a commercially available FAM-labeled anti-ASGPR antibody. In contrast, EGFP and all other control conjugates without the GalNAc side group displayed essentially no uptake in both cell lines (Figure 3A). Moreover, the results of the competitive flow cytometry experiments, in which EGFP-*p*(C2GalNAc) was coincubated with various designated inhibitors, indicated that the uptake of EGFP-*p*(C2GalNAc) by HepG2 was strongly inhibited by GalNAc and *p*(C2GalNAc), but not GlcNAc and *p*(GlcNAc) (Figures 3B and S18). More specifically, the polymeric *p*(C2GalNAc) was ∼100-fold more effective in diminishing the cellular uptake of EGFP-*p*(C2GalNAc) than the small molecular inhibitor GalNAc (Figure 3B), a phenomenon in line with the multivalent binding pattern of GalNAc and ASGPR. Of note, neither of the conjugates nor EGFP itself showed observable cytotoxicity in the tested concentration ranging from 50 to 14,000 nM (Figures S19 and 20). Together, the above results confirmed that the conjugation of GalNAc-functionalized PDS led to cell-selective uptake of the protein cargo.

Matile et al. previously reported the cell-membrane-penetrating effect of PDS through the proposed thiol−disulfide exchange reactions.[73,74] To investigate the role of the PDS backbone of EGFP-*p*(C2GalNAc) in the uptake by HepG2, we preblocked the thiol groups on the cell surface with various thiol-reactive agents for 30 min. It was found that all of the reagents, namely, iodoacetamide (IAM), 5,5′-dithiobis (2-nitrobenzoic acid) (DTNB), and maleimide, exhibited modest-to-high levels of inhibition on the cellular uptake of EGFP-

https://doi.org/10.1021/jacs.3c11914
J. Am. Chem. Soc. 2024, 146, 3974−3983

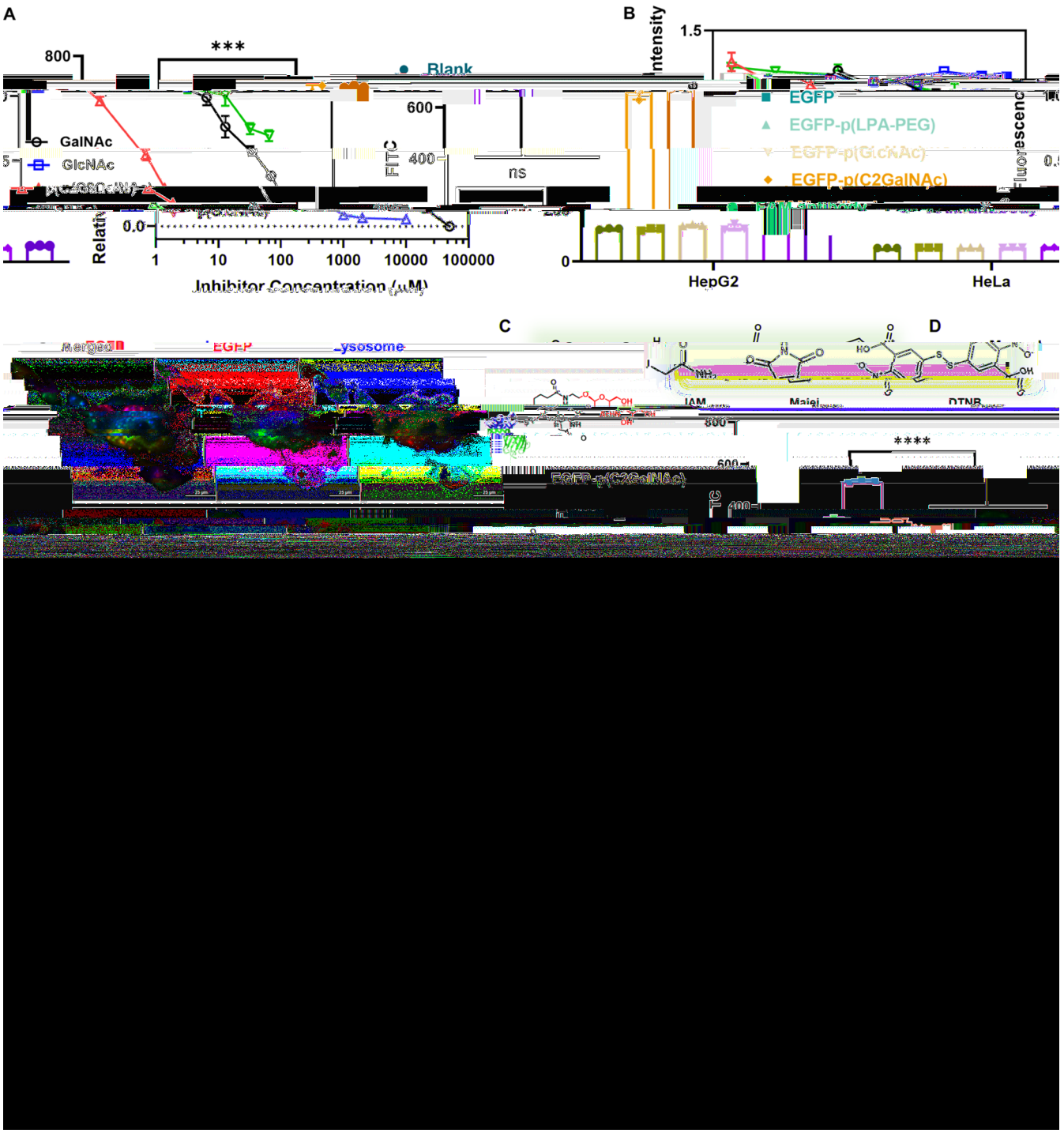

Figure 3. *In vitro* HepG2 cell-selective delivery. (A) Intracellular delivery of 1000 nM EGFP and various conjugates (EGFP-*p*(LPA-PEG), EGFP-*p*(GlcNAc), and EGFP-*p*(C2GalNAc)) into HepG2 or HeLa cells. (B) Plots of the concentration-dependent inhibitory effect of GalNAc, GlcNAc, *p*(C2GalNAc), and *p*(GlcNAc) on the delivery efficiency of 1000 nM EGFP-*p*(C2GalNAc) into HepG2 cells. (C) Inhibition of the delivery of 1000 nM EGFP-*p*(C2GalNAc) to HepG2 cells by various thiol-reactive agents: iodoacetamide (1 mM), DTNB (1 mM), or maleimide (50 μM). The intracellular delivery was assessed via EGFP fluorescence in flow cytometry. (D) CLSM images of HepG2 cells incubated with 1000 nM EGFP-*p*(C2GalNAc) or EGFP-*p*(GlcNAc). Green: EGFP and red: lysosome. (E) Proposed cell uptake pathway of EGFP-*p*(C2GalNAc). Data are presented as the mean ± SD. *p* Value was determined by the unpaired *t* test analysis: *** $p < 0.001$ and **** $p < 0.0001$.

p(C2GalNAc), echoing the findings of Matile et al. (Figure 3C).

We then performed confocal laser scanning microscopy (CLSM) to verify the targeted intracellular delivery of the conjugate EGFP-*p*(C2GalNAc), with EGFP-*p*(GlcNAc) as the control group for comparison. Strong EGFP fluorescence signal was observed for HepG2 cells incubated with EGFP-*p*(C2GalNAc) but not EGFP-*p*(GlcNAc) (Figure 3D). Importantly, a large portion of the green fluorescence signals were smeared within the cells and did not colocalize with the lysosome, confirming the cytosolic delivery of EGFP-*p*(C2GalNAc).

https://doi.org/10.1021/jacs.3c11914
J. Am. Chem. Soc. 2024, 146, 3974−3983

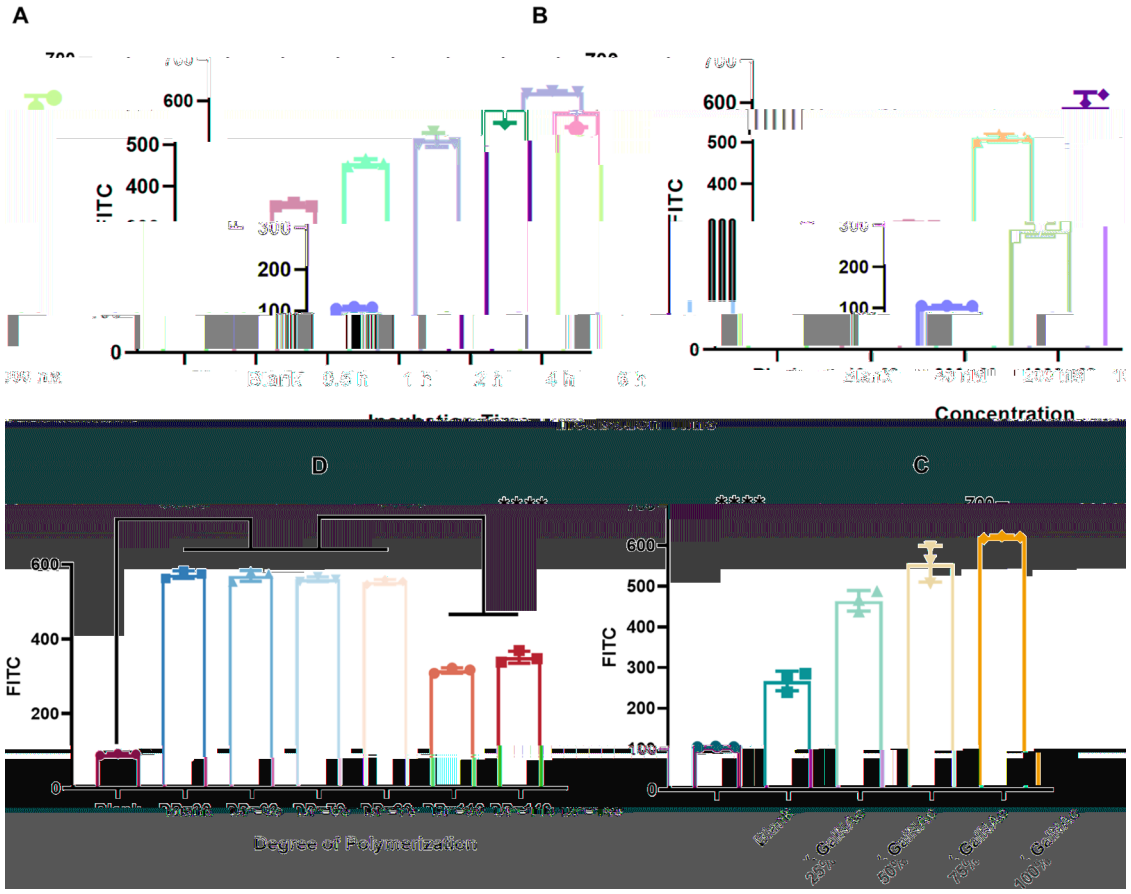

Figure 4. Optimization of the intracellular delivery of EGFP-*p*(C2GalNAc) into HepG2 cells under different conditions: (A) conjugate concentration, (B) incubation time, (C) GalNAc ratio, and (D) degree of polymerization. Data are presented as mean ± SD. *p* Value was determined by the unpaired *t* test analysis: **** $p < 0.0001$.

Combining all of the findings, we proposed the following plausible cellular uptake pathway (Figure 3E): In HepG2 cells overexpressing ASGPR, EGFP-*p*(C2GalNAc) swiftly adhered to and immobilized itself on the cell surface through the interaction between the GalNAc ligand and ASGPR (Figure 3A,B). In close proximity to the reactive thiol groups present on the cell surface, the anchored conjugate was then internalized via the previously reported thiol−disulfide exchange reactions (Figure 3C).[60] Conversely, for other cells with low ASGPR expression, such as HeLa cells, the internalization process was hindered (Figure 3A) as the bulky conjugate failed to anchor itself effectively onto the cell surface, thus unable to initiate effective of thiol−disulfide exchange reactions. This hypothesis was further supported by the observation that both EGFP-*p*(GlcNAc) and EGFP-*p*(LPA-PEG) displayed minimal cellular uptake in both HepG2 and HeLa cells (Figure 3A). Of note, the conventional GalNAc-ASGPR-mediated endocytosis pathway was not inhibited but coexisted as an additional internalization route, as dotted green fluorescence was still visible (Figure 3D) and blocking of thiol−disulfide exchange did not completely shut down the internalization of conjugates (Figure 3C). Collectively, our cellular uptake results underscored the significance of close spatial contact as a previously overlooked prerequisite for PDS-mediated penetration. Presumably, for PDS with substantial bulky side chains, in the absence of selective ligand recognition (e.g., GalNAc-ASGPR) or non-selective adsorption (e.g., polycations interacting with the cell membrane) to facilitate the attachment of the polymer to the cell surfaces, the bulky side chains could shield the PDS backbone, impeding thiol−disulfide exchange reactions and thereby hindering cellular internalization.

Having verified the hepatic targeting ability of the GalNAc-functionalized conjugates, we continued to explore optimal conditions for the maximized delivery efficiency of EGFP-*p*(C2GalNAc). The targeting effect was observed when HepG2 cells were incubated with EGFP-*p*(C2GalNAc) at 40 mM, and a monotone increase of the cellular uptake was seen as the concentration of EGFP-*p*(C2GalNAc) was raised to 1000 mM (Figure 4A). Furthermore, the level of conjugate internalization increased gradually with incubation time and reached equilibrium between 2 and 4 h (Figure 4B). The effect of the GalNAc ratio in the PDS on the delivery efficiency was also investigated by copolymerizing LPA-GlcNAc and LPA-C2GalNAc monomers at different ratios, which, as expected, gave greater internalization as the ratio of LPA-C2GalNAc became higher (Figures 4C and S21). Previous studies have highlighted the linker length and flexibility on the GalNAc-ASGPR binding;[57] therefore, we also investigated the effect of link on the delivery efficiency. Four GalNAc-functionalized conjugates with similar apparent molecular weights (EGFP-*p*(C2GalNAc), EGFP-*p*(C3GalNAc), EGFP-*p*(EG2GalNAc), and EGFP-*p*(EG3GalNAc)) were made and found to be delivered into HepG2 cells with comparable efficiencies (Figure S22).

https://doi.org/10.1021/jacs.3c11914
J. Am. Chem. Soc. 2024, 146, 3974−3983

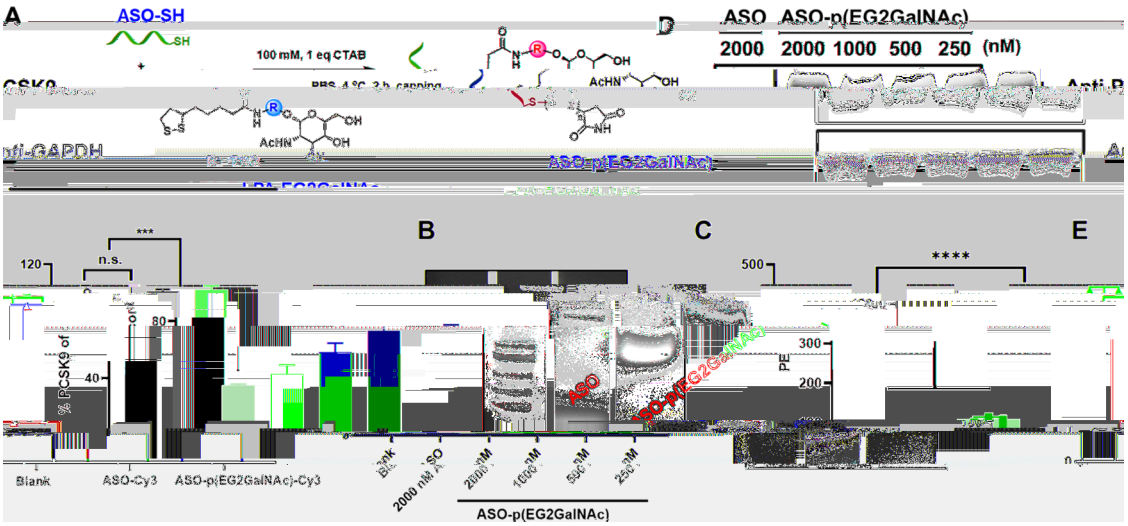

Figure 5. Synthesis and intracellular delivery of ASO-*p*(EG2GalNAc) for *in vitro* PCSK9 inhibition. (A) Scheme of the ASO-SH-initiated polymerization of LPA-EG2-GalNAc. (B) Agarose gel electrophoresis characterization of the resulting conjugate ASO-*p*(EG2GalNAc). (C) Fluorescence of Cy3-labeled ASO and ASO-*p*(EG2GalNAc) in HepG2 cells using flow cytometry. (D) Western blot analysis of PCSK9 knockdown by ASO-*p*(EG2GalNAc) in HepG2 cells. (E) Quantitative analysis of the inhibition efficiency of ASO-*p*(EG2GalNAc) based on 2 independent repeats. Data are presented as mean ± SD. *p* Value was determined by the unpaired *t* test analysis: *** $p < 0.001$ and **** $p < 0.0001$.

Next, the DP of *p*(LPA-C2GalNAc) (30, 60, 70, 90, 110, and 140), which was controlled by simply varying the reaction time, was tuned in the EGFP-*p*(C2GalNAc) conjugates to probe the size effect. Interestingly, for the conjugates with a DP of *p*(LPA-C2GalNAc) of 90 or smaller, no significant difference in the cellular uptake level was detected. We reasoned that, as only trivalent GalNAc was needed to bind ASGPR, a DP of 30 or above would be sufficiently long to offer equally strong binding for targeting. However, when the DP of *p*(LPA-C2GalNAc) was increased to 110 or 140, the delivery efficiency of the conjugates decreased significantly (Figures 4D and S23). A similar trend was observed for the delivery results of another GalNAc-functionalized conjugate, EGFP-*p*(EG3-GalNAc) (Figures S24 and 25). We reasoned that while a higher DP of PDS was unlikely to affect the binding of the conjugate to ASGPR, the larger size of the conjugate would likely jeopardize the subsequent PDS-mediated membrane penetration. According to the proposed cell internalization routes, close proximity was required for the on-surface thiol−disulfide exchange (Figure 3E), and unnecessarily long *p*(LPA-C2GalNAc) would probably increase the distance of the terminal cargo to the cell membrane statistically. Consequently, the portion of noneffective thiol−disulfide exchange, i.e., premature cargo release due to PDS depolymerization, and failed internalization due to the large size would be more pronounced for those PDS with DP of greater than a certain size.

Motived by the successful conjugation of proteins, we were then encouraged to test whether the same strategy could be expanded to ASO, a class of important oligonucleotide (OND) drugs. Our initial attempts to polymerize LPA-EG2GalNAc using a thiol-tethered oligonucleotide (ASO-SH) as an initiator, unfortunately, were found unsuccessful when following the condition for making the EGFP conjugate. We tentatively attributed the failed synthesis to the high negative charge density of ASO, which prevented effective contact of the initiator with the monomer aggregates.[75] To test this hypothesis and solve the problem, we screened a few cationic surfactants and found that adding cetyltrimethylammonium bromide (CTAB) into the ROP system was effective in generating the desired ASO conjugates. Agarose gel electrophoresis of the reaction mixture found the disappearance of the ASO-SH band, along with a new band appeared at the higher MW region attributable to the corresponding ASO-PDS conjugate (Figure 5A,B). Presumably, the use of CTAB increased the lipophilicity of ASO-SH, which was beneficial in bringing the monomers and the macroinitiator together for ROP.

The intracellular delivery efficiency of ASO-*p*(EG2GalNAc) in HepG2 cells was then investigated. Cy3-maleimide was covalently linked to both ASO-SH and ASO-*p*(EG2GalNAc), and the fluorescence intensity in HepG2 cells was analyzed by flow cytometry. The results showed that free ASO-Cy3 of 10 nM was barely taken up by HepG2 cells, with no significant difference compared to that of the blank control group. In contrast, HepG2 cells treated with the same concentration of ASO-*p*(EG2GalNAc) conjugate exhibited significantly increased fluorescence intensity (Figure 5C). Subsequently, we investigated whether the ASO was indeed delivered into the cytosol to execute its biological function. For this, we selected proprotein convertase subtilisin-kexin type 9 (PCSK9), a common therapeutic target in hepatic metabolic disorders, as our target. PCSK9 is a serine protease that significantly reduces the low-density lipoprotein receptor (LDLR) on liver cells, affecting the metabolism and clearance of low-density lipoprotein cholesterol (LDL-C) in the bloodstream.[76] Elevated PCSK9 accelerates the clearance of LDLR on the cell surface, leading to increased cholesterol levels in the blood and risk of various cardiovascular diseases.[77] Here, we constructed a thiol-tethered anti-PCSK9 ASO with the sequence obtained from previous studies,[78] and successfully prepared the conjugate. HepG2 cells were treated with ASO-*p*(EG2GalNAc) at different concentrations, and the intracellular PCSK9 levels were analyzed by Western blotting after 24 h of treatment. The results showed ASO-*p*(EG2GalNAc) dose-dependent reduction in the PCSK9 protein level, with approximately 70% knockdown at 2000 nM ASO-*p*(EG2GalNAc) (Figures 5D,E and S26). In contrast, treatment of the

https://doi.org/10.1021/jacs.3c11914
J. Am. Chem. Soc. 2024, 146, 3974−3983

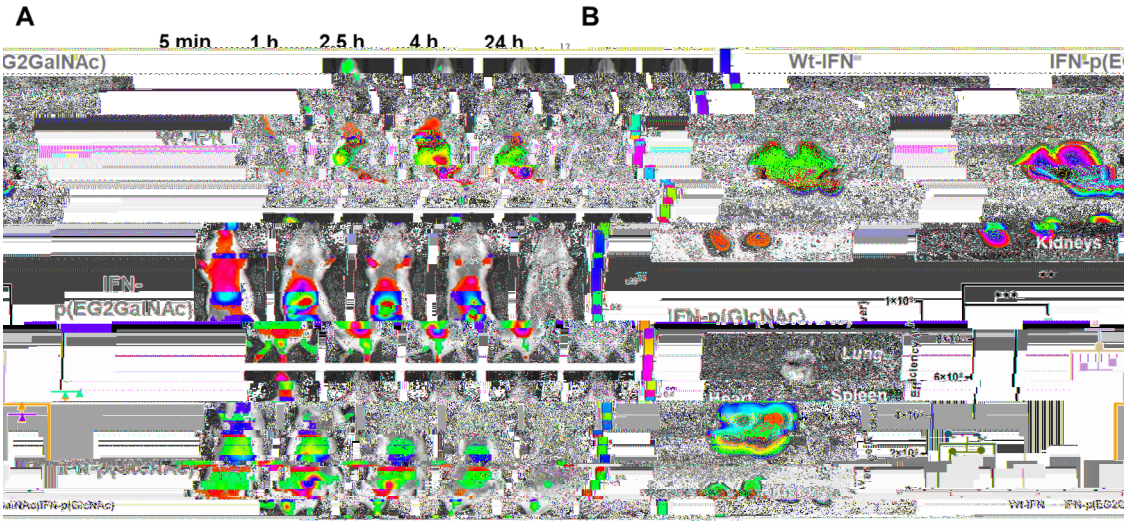

Figure 6. *In vivo* hepatocyte delivery. (A) Fluorescent images of live animals at different time points. The Cy5-modified IFN conjugates or IFN (20 μg) was *i.v.* infused into female balb/c mice (20 g) via tail vein and monitored with a live animal fluorescence imaging system. (B) Fluorescent images of the extracted organs at 24 h and quantification of the average radiant efficiency of the liver. Data are presented as mean ± SD. p Value was determined by the unpaired t test analysis: ** $p < 0.01$ and *** $p < 0.001$.

cells with free ASO at the same concentration did not affect intracellular PCSK9 levels. This result unambiguously demonstrated the successful intracellular delivery of ASO-p(EG2GalNAc) into HepG2 cells with retained biological functions. Considering that we used an ASO with no chemical modifications on the oligonucleotide backbone,[46,79] there is likely plenty of room for potency optimization using this p(EG2GalNAc) conjugation strategy once state-of-the-art modification technologies were employed to the ASO.

To validate the liver-targeted delivery *in vivo*, we prepared a model conjugate of interferon (IFN) and PDS composed of LPA-EG2GalNAc. Briefly, an IFN mutant with a reactive cysteine was used to initiate the ROP of LPA-EG2GalNAc to yield the corresponding conjugate IFN-p(EG2GalNAc). The conjugate IFN-p(GlcNAc) and pristine IFN were selected as negative control groups (Figure S27). All of the groups were modified with a fluorescent dye Cy5, and the mice were closely monitored with fluorescence imaging in the first 4 h and sacrificed at 24 h. Live animal imaging at different time points showed that the fluorescent signal of IFN-p(EG2GalNAc) accumulated in the liver immediately upon injection (5 min), growing rapidly and reaching the maximized liver signal at ∼2.5 h. Interestingly, the signal slowly decreased after 4 h (Figure 6A), which could be attributed to the PDS depolymerization in the liver, the organ known to contain a high GSH concentration. Despite the live animal imaging showing almost no fluorescent signal at 24 h, the extracted organ fluorescence imaging still showed a significant liver enrichment effect for IFN-p(EG2GalNAc) over the other two groups (Figure 6B). Overall, the *in vivo* imaging study demonstrated the potential of this conjugate for targeted delivery of biologics to the liver.

CONCLUSIONS

The polymerization of bulky lipoic acid derivatives has posed a significant challenge in the past. In this study, we successfully overcome this obstacle by harnessing the AIP effect. This innovative approach enabled us to achieve the ROP of several glycol-functionalized lipoamide monomers initiated by thiol-functionalized proteins and ASOs. Consequently, we produced site-specific protein/ASO-PDS conjugates with remarkably narrow dispersity. Among these conjugates, GalNAc-functionalized PDS has exhibited selective intracellular delivery of biologics into hepatocytes with retained functions both *in vitro* and *in vivo*. This selectivity arises from a synergistic interplay between GalNAc-ASGPR binding, which mediates precise cell targeting, and on-surface thiol−disulfide exchange for efficient cell internalization. Our findings underscore the critical role played by the close proximity of the PDS backbone to the cell surface, a factor that had previously been overlooked, in orchestrating the successful thiol−disulfide exchange and subsequent cellular penetration. It is important to note that while liver targeting has been pursued through various strategies in the past, many of these approaches encountered clearance by Kupffer cells in the liver or faced challenges with low endosomal escape efficiency. In the future, this versatile platform could be further empowered by incorporating various functional groups into the side chain of a PDS for tailored properties and biological functions. Notably examples include but are not limited to conjugating amphiphilic cell-penetrating and cell-targeting PDS for self-assembly, adding stimuli-sensitive side chains for tumor-microenvironment responsiveness and modulation, and integrated theranostics. These newly developed conjugates hold immense promise in surmounting the complex biological barriers encountered during systemic and cell-selective delivery of biomacromolecular cargos. The study represents a significant advancement in the field and offers exciting possibilities for the diagnosis and treatment of various liver-targeting diseases.

ASSOCIATED CONTENT

Supporting Information

The Supporting Information is available free of charge at https://pubs.acs.org/doi/10.1021/jacs.3c11914.

Full details of the synthesis, experimental methods, and characterizations; sequences of proteins in the article; synthetic procedures of LPA-*R*-GalNAc; typical conditions for the ROP of LPA-R-GalNAc; synthesis of the conjugate ASO-p(EG2GalNAc); flow cytometry analysis

https://doi.org/10.1021/jacs.3c11914
J. Am. Chem. Soc. 2024, 146, 3974−3983

of cellular delivery; cellular internalization measured by CLSM; Western blot analysis of PCSK9 knockdown by ASO-*p*(EG2GalNAc) conjugates; synthesis of Cy5-labeled IFN conjugates or IFN; *in vivo* biodistribution of Cy5-labeled IFN conjugates or IFN; ^{1}H NMR spectrum of LPA-NHS, LPA-C2OH, LPA-C3GalNAc, LPA-EG2GalNAc, and LPA-GlcNAc; ^{13}C NMR spectrum of LPA-C2GalNAc, LPA-C3GalNAc, LPA-EG2-GalNAc, and LPA-GlcNAc; mass spectrometry of LPA-C2GalNAc, LPA-C3GalNAc, LPA-EG2GalNAc, and LPA-GlcNAc; DLS of 50 and 100 mM LPA-EG2GalNAc; overlay of the ^{1}H NMR spectra of monomer LPA-C2GalNAc and 2-mercaptoethanesulfonate-initiated polymer *p*(C2GalNAc); cell livability rate of HepG2 cells with the concentration of EGFP-*p*(C2GalNAc) and EGFP-*p*(GlcNAc); intracellular delivery of EGFP-*p*(C2GalNAc), EGFP-*p*(C3GalNAc), EGFP-*p*(EG2GalNAc), or EGFP-*p*(EG3GalNAc) into HepG2 cells; biological repeat of Western blot analysis of PCSK9 knockdown by ASO-*p*(EG2GalNAc) in HepG2 cells; and nonreducing SDS-PAGE of IFN-*p*(EG2GalNAc), IFN-*p*(GlcNAc), Wt-IFN, EGFP-*p*(C2GalNAc) conjugates treated with various reducing agents, EGFP-polydisulfide conjugates by copolymerizing LPA-GlcNAc and LPA-C2GalNAc monomers at different ratios, EGFP-*p*(C2GalNAc) conjugates with different degrees of polymerization, and EGFP-*p*(EG3-GalNAc) conjugates with different degrees of polymerization (PDF)

AUTHOR INFORMATION

Corresponding Author

Hua Lu − *Beijing National Laboratory for Molecular Sciences, Center for Soft Matter Science and Engineering, Key Laboratory of Polymer Chemistry and Physics of Ministry of Education, College of Chemistry and Molecular Engineering, Peking University, Beijing 100871, People's Republic of China;* orcid.org/0000-0003-2180-3091; Email: chemhualu@pku.edu.cn

Authors

Jianhua Lu − *Beijing National Laboratory for Molecular Sciences, Center for Soft Matter Science and Engineering, Key Laboratory of Polymer Chemistry and Physics of Ministry of Education, College of Chemistry and Molecular Engineering, Peking University, Beijing 100871, People's Republic of China;* orcid.org/0009-0001-5592-2622

Yuanhao Dai − *Beijing National Laboratory for Molecular Sciences, Center for Soft Matter Science and Engineering, Key Laboratory of Polymer Chemistry and Physics of Ministry of Education, College of Chemistry and Molecular Engineering, Peking University, Beijing 100871, People's Republic of China*

Yahui He − *Beijing National Laboratory for Molecular Sciences, Center for Soft Matter Science and Engineering, Key Laboratory of Polymer Chemistry and Physics of Ministry of Education, College of Chemistry and Molecular Engineering, Peking University, Beijing 100871, People's Republic of China*

Ting Zhang − *Department of Microbiology & Infectious Disease Center, Peking University Health Science Center, Beijing 100191, People's Republic of China*

Jing Zhang − *Department of Microbiology & Infectious Disease Center, Peking University Health Science Center, Beijing 100191, People's Republic of China*

Xiangmei Chen − *Department of Microbiology & Infectious Disease Center, Peking University Health Science Center, Beijing 100191, People's Republic of China*

Changtao Jiang − *Department of Immunology, School of Basic Medical Sciences, State Key Laboratory of Female Fertility Promotion, Peking University, Beijing 100191, China;* orcid.org/0000-0002-5206-2372

Complete contact information is available at: https://pubs.acs.org/10.1021/jacs.3c11914

Notes

The authors declare no competing financial interest.

ACKNOWLEDGMENTS

This work was supported by the National Key Research and Development Program of China (2019YFA0904203), National Natural Science Foundation of China (22125101), and Beijing Natural Science Foundation (2220023).

REFERENCES

(1) Kong, H. J.; Mooney, D. J. Microenvironmental regulation of biomacromolecular therapies. *Nat. Rev. Drug Discovery* **2007**, *6* (6), 455−463.

(2) Adeyemi, S. A.; Choonara, Y. E. Current advances in cell therapeutics: a biomacromolecules application perspective. *Expert Opin. Drug Delivery* **2022**, *19* (5), 521−538.

(3) Du, A. W.; Stenzel, M. H. Drug Carriers for the Delivery of Therapeutic Peptides. *Biomacromolecules* **2014**, *15* (4), 1097−1114.

(4) Tian, Y.; Tirrell, M. V.; LaBelle, J. L. Harnessing the Therapeutic Potential of Biomacromolecules through Intracellular Delivery of Nucleic Acids, Peptides, and Proteins. *Adv. Healthcare Mater.* **2022**, *11* (12), No. 2102600, DOI: 10.1002/adhm.202102600.

(5) Eygeris, Y.; Gupta, M.; Kim, J.; Sahay, G. Chemistry of Lipid Nanoparticles for RNA Delivery. *Acc. Chem. Res.* **2022**, *55* (1), 2−12.

(6) Datta, L. P.; Manchineella, S.; Govindaraju, T. Biomolecules-derived biomaterials. *Biomaterials* **2020**, *230*, 119633−119673.

(7) Hou, Y.; Zhou, Y.; Wang, H.; Wang, R.; Yuan, J.; Hu, Y.; Sheng, K.; Feng, J.; Yang, S.; Lu, H. Macrocyclization of interferon-poly(alpha-amino acid) conjugates significantly improves the tumor retention, penetration, and antitumor efficacy. *J. Am. Chem. Soc.* **2018**, *140* (3), 1170−1178.

(8) Whitehead, K. A.; Langer, R.; Anderson, D. G. Knocking down barriers: advances in siRNA delivery. *Nat. Rev. Drug Discovery* **2009**, *8* (2), 129−138.

(9) Antosova, Z.; Mackova, M.; Kral, V.; Macek, T. Therapeutic application of peptides and proteins: parenteral forever? *Trends Biotechnol.* **2009**, *27* (11), 628−635.

(10) Fang, H.; Sha, Y.; Yang, L.; Jiang, J.; Yin, L.; Li, J.; Li, B.; Klumperman, B.; Zhong, Z.; Meng, F. Macrophage-Targeted Hydroxychloroquine Nanotherapeutics for Rheumatoid Arthritis Therapy. *ACS Appl. Mater. Interfaces* **2022**, *14* (7), 8824−8837.

(11) Zhang, Q.; Liu, Y.; Fei, Y.; Xie, J.; Zhao, X.; Zhong, Z.; Deng, C. Phenylboronic Acid-Functionalized Copolypeptides: Facile Synthesis and Responsive Dual Anticancer Drug Release. *Biomacromolecules* **2022**, *23* (7), 2989−2998.

(12) Dilliard, S. A.; Cheng, Q.; Siegwart, D. J. On the mechanism of tissue-specific mRNA delivery by selective organ targeting nanoparticles. *Proc. Natl. Acad. Sci. U. S. A.* **2021**, *118* (52), No. e2109256118, DOI: 10.1073/pnas.2109256118.

(13) Wang, X.; Liu, S.; Sun, Y.; Yu, X.; Lee, S. M.; Cheng, Q.; Wei, T.; Gong, J.; Robinson, J.; Zhang, D.; Lian, X.; Basak, P.; Siegwart, D. J. Preparation of selective organ-targeting (SORT) lipid nanoparticles

(LNPs) using multiple technical methods for tissue-specific mRNA delivery. *Nat. Protoc.* **2023**, *18* (1), 265−291.
(14) Wang, H.; Wang, R.; Cai, K.; He, H.; Liu, Y.; Yen, J.; Wang, Z.; Xu, M.; Sun, Y.; Zhou, X.; Yin, Q.; Tang, L.; Dobrucki, I. T.; Dobrucki, L. W.; Chaney, E. J.; Boppart, S. A.; Fan, T. M.; Lezmi, S.; Chen, X.; Yin, L.; Cheng, J. Selective *in vivo* metabolic cell-labeling-mediated cancer targeting. *Nat. Chem. Biol.* **2017**, *13* (4), 415−424.
(15) Sefah, K.; Shangguan, D.; Xiong, X.; O'Donoghue, M. B.; Tan, W. Development of DNA aptamers using Cell-SELEX. *Nat. Protoc.* **2010**, *5* (6), 1169−1185.
(16) Yu, R. Z.; Gunawan, R.; Post, N.; Zanardi, T.; Hall, S.; Burkey, J.; Kim, T.-W.; Graham, M. J.; Prakash, T. P.; Seth, P. P.; Swayze, E. E.; Geary, R. S.; Henry, S. P.; Wang, Y. Disposition and Pharmacokinetics of a GalNAc3-Conjugated Antisense Oligonucleotide Targeting Human Lipoprotein (a) in Monkeys. *Nucleic Acid Ther.* **2016**, *26* (6), 372−380.
(17) Huang, Y. Preclinical and clinical advances of GalNAc-decorated nucleic acid therapeutics. *Mol. Ther.–Nucleic Acids* **2017**, *6*, 116−132.
(18) Zimmermann, T. S.; Karsten, V.; Chan, A.; Chiesa, J.; Boyce, M.; Bettencourt, B. R.; Hutabarat, R.; Nochur, S.; Vaishnaw, A.; Gollob, J. Clinical proof of concept for a novel hepatocyte-targeting GalNAc-siRNA conjugate. *Mol. Ther.* **2017**, *25* (1), 71−78.
(19) Janas, M. M.; Schlegel, M. K.; Harbison, C. E.; Yilmaz, V. O.; Jiang, Y.; Parmar, R.; Zlatev, I.; Castoreno, A.; Xu, H.; Shulga-Morskaya, S.; Rajeev, K. G.; Manoharan, M.; Keirstead, N. D.; Maier, M. A.; Jadhav, V. Selection of GalNAc-conjugated siRNAs with limited off-target-driven rat hepatotoxicity. *Nat. Commun.* **2018**, *9* (1), No. 723, DOI: 10.1038/s41467-018-02989-4.
(20) Springer, A. D.; Dowdy, S. F. GalNAc-siRNA conjugates: leading the way for delivery of RNAi therapeutics. *Nucleic Acid Ther.* **2018**, *28* (3), 109−118.
(21) Wang, Y.; Yu, R. Z.; Henry, S.; Geary, R. S. Pharmacokinetics and clinical pharmacology considerations of GalNAc3-conjugated antisense oligonucleotides. *Expert Opin. Drug Metab. Toxicol.* **2019**, *15* (6), 475−485.
(22) Tong, P.-H.; Zhu, L.; Zang, Y.; Li, J.; He, X.-P.; James, T. D. Metal−organic frameworks (MOFs) as host materials for the enhanced delivery of biomacromolecular therapeutics. *Chem. Commun.* **2021**, *57* (91), 12098−12110.
(23) Sun, Y.; Lau, S. Y.; Lim, Z. W.; Chang, S. C.; Ghadessy, F.; Partridge, A.; Miserez, A. Phase-separating peptides for direct cytosolic delivery and redox-activated release of macromolecular therapeutics. *Nat. Chem.* **2022**, *14* (3), 274−283.
(24) Evans, B. C.; Fletcher, R. B.; Kilchrist, K. V.; Dailing, E. A.; Mukalel, A. J.; Colazo, J. M.; Oliver, M.; Cheung-Flynn, J.; Brophy, C. M.; Tierney, J. W.; Isenberg, J. S.; Hankenson, K. D.; Ghimire, K.; Lander, C.; Gersbach, C. A.; Duvall, C. L. An anionic, endosome-escaping polymer to potentiate intracellular delivery of cationic peptides, biomacromolecules, and nanoparticles. *Nat. Commun.* **2019**, *10* (1), No. 5012, DOI: 10.1038/s41467-019-12906-y.
(25) Kanasty, R.; Dorkin, J. R.; Vegas, A.; Anderson, D. Delivery materials for siRNA therapeutics. *Nat. Mater.* **2013**, *12* (11), 967−977.
(26) Riley, R. S.; June, C. H.; Langer, R.; Mitchell, M. J. Delivery technologies for cancer immunotherapy. *Nat. Rev. Drug Discovery* **2019**, *18* (3), 175−196.
(27) Hou, X.; Zaks, T.; Langer, R.; Dong, Y. Lipid nanoparticles for mRNA delivery. *Nat. Rev. Mater.* **2021**, *6* (12), 1078−1094.
(28) Zhu, Y. W.; Lin, M. Y.; Hu, W. T.; Wang, J. K.; Zhang, Z. G.; Zhang, K.; Yu, B. R.; Xu, F. J. Controllable Disulfide Exchange Polymerization of Polyguanidine for Effective Biomedical Applications by Thiol-Mediated Uptake. *Angew. Chem., Int. Ed.* **2022**, *61* (23), No. e202200535, DOI: 10.1002/anie.202200535.
(29) Mu, S.; Zhu, Y.; Wang, Y.; Qu, S.; Huang, Y.; Zheng, L.; Duan, S.; Yu, B.; Qin, M.; Xu, F. J. Cationic Polysaccharide Conjugates as Antibiotic Adjuvants Resensitize Multidrug-Resistant Bacteria and Prevent Resistance. *Adv. Mater.* **2022**, *34* (41), No. 2204065, DOI: 10.1002/adma.202204065.
(30) Tan, X.; Jia, F.; Wang, P.; Zhang, K. Nucleic acid-based drug delivery strategies. *J. Controlled Release* **2020**, *323*, 240−252.
(31) Wang, D.; Wang, Q.; Wang, Y.; Chen, P.; Lu, X.; Jia, F.; Sun, Y.; Sun, T.; Zhang, L.; Che, F.; He, J.; Lian, L.; Morano, G.; Shen, M.; Ren, M.; Dong, S. S.; Zhao, J. J.; Zhang, K. Targeting oncogenic KRAS with molecular brush-conjugated antisense oligonucleotides. *Proc. Natl. Acad. Sci. U. S. A.* **2022**, *119* (29), No. e2113180119, DOI: 10.1073/pnas.2113180119.
(32) Lu, X.; Fu, H.; Shih, K.-C.; Jia, F.; Sun, Y.; Wang, D.; Wang, Y.; Ekatan, S.; Nieh, M.-P.; Lin, Y.; Zhang, K. DNA-Mediated Step-Growth Polymerization of Bottlebrush Macromonomers. *J. Am. Chem. Soc.* **2020**, *142* (23), 10297−10301.
(33) Wang, Y.; Wang, D.; Jia, F.; Miller, A.; Tan, X.; Chen, P.; Zhang, L.; Lu, H.; Fang, Y.; Kang, X.; Cai, J.; Ren, M.; Zhang, K. Self-Assembled DNA−PEG Bottlebrushes Enhance Antisense Activity and Pharmacokinetics of Oligonucleotides. *ACS Appl. Mater. Interfaces* **2020**, *12* (41), 45830−45837.
(34) Fischer, D.; Li, Y.; Ahlemeyer, B.; Krieglstein, J.; Kissel, T. *In vitro* cytotoxicity testing of polycations: influence of polymer structure on cell viability and hemolysis. *Biomaterials* **2003**, *24* (7), 1121−1131.
(35) Chaudhary, N.; Weissman, D.; Whitehead, K. A. mRNA vaccines for infectious diseases: principles, delivery and clinical translation. *Nat. Rev. Drug Discovery* **2021**, *20* (11), 817−838.
(36) Vargason, A. M.; Anselmo, A. C.; Mitragotri, S. The evolution of commercial drug delivery technologies. *Nat. Biomed. Eng.* **2021**, *5* (9), 951−967.
(37) Rennick, J. J.; Johnston, A. P. R.; Parton, R. G. Key principles and methods for studying the endocytosis of biological and nanoparticle therapeutics. *Nat. Nanotechnol.* **2021**, *16* (3), 266−276.
(38) Qiu, M.; Tang, Y.; Chen, J.; Muriph, R.; Ye, Z.; Huang, C.; Evans, J.; Henske, E. P.; Xu, Q. Lung-selective mRNA delivery of synthetic lipid nanoparticles for the treatment of pulmonary lymphangioleiomyomatosis. *Proc. Natl. Acad. Sci. U. S. A.* **2022**, *119* (8), No. e2116271119, DOI: 10.1073/pnas.2116271119.
(39) Zhao, Z.; Liu, X.; Hou, M.; Zhou, R.; Wu, F.; Yan, J.; Li, W.; Zheng, Y.; Zhong, Q.; Chen, Y.; Yin, L. Endocytosis-Independent and Cancer-Selective Cytosolic Protein Delivery via Reversible Tagging with LAT1 substrate. *Adv. Mater.* **2022**, *34* (35), No. 2110560, DOI: 10.1002/adma.202110560.
(40) Liu, C.; Wan, T.; Wang, H.; Zhang, S.; Ping, Y.; Cheng, Y. A boronic acid−rich dendrimer with robust and unprecedented efficiency for cytosolic protein delivery and CRISPR-Cas9 gene editing. *Sci. Adv.* **2019**, *5* (6), No. eaaw8922, DOI: 10.1126/sciadv.aaw8922.
(41) Liu, J.; Luo, T.; Xue, Y.; Mao, L.; Stang, P. J.; Wang, M. Hierarchical Self-assembly of Discrete Metal−Organic Cages into Supramolecular Nanoparticles for Intracellular Protein Delivery. *Angew. Chem., Int. Ed.* **2021**, *60* (10), 5429−5435.
(42) Raguram, A.; Banskota, S.; Liu, D. R. Therapeutic *in vivo* delivery of gene editing agents. *Cell* **2022**, *185* (15), 2806−2827.
(43) Zhang, Q.; Deng, Y. X.; Luo, H. X.; Shi, C. Y.; Geise, G. M.; Feringa, B. L.; Tian, H.; Qu, D. H. Assembling a natural small molecule into a supramolecular network with high structural order and dynamic functions. *J. Am. Chem. Soc.* **2019**, *141* (32), 12804−12814.
(44) Yin, L.; Tang, H.; Kim, K. H.; Zheng, N.; Song, Z.; Gabrielson, N. P.; Lu, H.; Cheng, J. Light-Responsive Helical Polypeptides Capable of Reducing Toxicity and Unpacking DNA: Toward Nonviral Gene Delivery. *Angew. Chem., Int. Ed.* **2013**, *52* (35), 9182−9186.
(45) O'Brien, K.; Breyne, K.; Ughetto, S.; Laurent, L. C.; Breakefield, X. O. RNA delivery by extracellular vesicles in mammalian cells and its applications. *Nat. Rev. Mol. Cell Biol.* **2020**, *21* (10), 585−606.
(46) Roberts, T. C.; Langer, R.; Wood, M. J. A. Advances in oligonucleotide drug delivery. *Nat. Rev. Drug Discovery* **2020**, *19* (10), 673−694.
(47) Li, C.; Samulski, R. J. Engineering adeno-associated virus vectors for gene therapy. *Nat. Rev. Genet.* **2020**, *21* (4), 255−272.

(48) Zhang, Q.; Shi, C. Y.; Qu, D. H.; Long, Y. T.; Feringa, B. L.; Tian, H. Exploring a naturally tailored small molecule for stretchable, self-healing, and adhesive supramolecular polymers. *Sci. Adv.* **2018**, *4* (7), No. eaat8192, DOI: 10.1126/sciadv.aat8192.
(49) Zhang, Q.; Qu, D.-H.; Feringa, B. L.; Tian, H. Disulfide-mediated reversible polymerization toward intrinsically dynamic smart materials. *J. Am. Chem. Soc.* **2022**, *144* (5), 2022−2033.
(50) Guo, J.; Zhang, S.; Tao, Y.; Fan, B.; Tang, W. Glutathione-triggered biodegradable poly(disulfide)s: ring-opening copolymerization and potent antibacterial activity. *Polym. Chem.* **2022**, *13* (48), 6637−6649.
(51) Zhou, Y.; Liang, Q.; Wu, X.; Duan, S.; Ge, C.; Ye, H.; Lu, J.; Zhu, R.; Chen, Y.; Meng, F.; Yin, L. siRNA Delivery against Myocardial Ischemia Reperfusion Injury Mediated by Reversibly Camouflaged Biomimetic Nanocomplexes. *Adv. Mater.* **2023**, *35* (23), No. 2210691, DOI: 10.1002/adma.202210691.
(52) Liu, X.; Zhao, Z.; Wu, F.; Chen, Y.; Yin, L. Tailoring Hyperbranched Poly(β-amino ester) as a Robust and Universal Platform for Cytosolic Protein Delivery. *Adv. Mater.* **2022**, *34* (8), No. 2108116, DOI: 10.1002/adma.202108116.
(53) Hou, M.; Wei, Y.; Zhao, Z.; Han, W.; Zhou, R.; Zhou, Y.; Zheng, Y.; Yin, L. Immuno-Engineered Nanodecoys for the Multi-Target Anti-Inflammatory Treatment of Autoimmune Diseases. *Adv. Mater.* **2022**, *34* (12), No. 2108817, DOI: 10.1002/adma.202108817.
(54) Kong, Y.; Zeng, K.; Zhang, Y.; Shao, J.; Yan, J.; Liao, J.-Y.; Wang, W.; Dai, X.; Weng, Q.; Yao, S. Q.; Zeng, S.; Qian, L. *In vivo* targeted delivery of antibodies into cancer cells with pH-responsive cell-penetrating poly(disulfide)s. *Chem. Commun.* **2022**, *58* (9), 1314−1317.
(55) Guo, J.; Wan, T.; Li, B.; Pan, Q.; Xin, H.; Qiu, Y.; Ping, Y. Rational Design of Poly(disulfide)s as a Universal Platform for Delivery of CRISPR-Cas9Machineries toward Therapeutic Genome Editing. *ACS Cent. Sci.* **2021**, *7* (6), 990−1000.
(56) Wang, H.-X.; Xiong, M.-H.; Wang, Y.-C.; Zhu, J.; Wang, J. N-acetylgalactosamine functionalized mixed micellar nanoparticles for targeted delivery of siRNA to liver. *J. Controlled Release* **2013**, *166* (2), 106−114.
(57) Nair, J. K.; Willoughby, J. L.; Chan, A.; Charisse, K.; Alam, M. R.; Wang, Q.; Hoekstra, M.; Kandasamy, P.; Kel'in, A. V.; Milstein, S.; Taneja, N.; O'Shea, J.; Shaikh, S.; Zhang, L.; van der Sluis, R. J.; Jung, M. E.; Akinc, A.; Hutabarat, R.; Kuchimanchi, S.; Fitzgerald, K.; Zimmermann, T.; van Berkel, T. J.; Maier, M. A.; Rajeev, K. G.; Manoharan, M. Multivalent N-acetylgalactosamine-conjugated siRNA localizes in hepatocytes and elicits robust RNAi-mediated gene silencing. *J. Am. Chem. Soc.* **2014**, *136* (49), 16958−16961.
(58) Dhande, Y. K.; Wagh, B. S.; Hall, B. C.; Sprouse, D.; Hackett, P. B.; Reineke, T. M. N-acetylgalactosamine block-co-polycations form stable polyplexes with plasmids and promote liver-targeted delivery. *Biomacromolecules* **2016**, *17* (3), 830−840.
(59) Bang, E. K.; Gasparini, G.; Molinard, G.; Roux, A.; Sakai, N.; Matile, S. Substrate-initiated synthesis of cell-penetrating poly(disulfide)s. *J. Am. Chem. Soc.* **2013**, *135* (6), 2088−2091.
(60) Gasparini, G.; Bang, E. K.; Molinard, G.; Tulumello, D. V.; Ward, S.; Kelley, S. O.; Roux, A.; Sakai, N.; Matile, S. Cellular uptake of substrate-initiated cell-penetrating poly(disulfide)s. *J. Am. Chem. Soc.* **2014**, *136* (16), 6069−6074.
(61) Laurent, Q.; Martinent, R.; Lim, B.; Pham, A.-T.; Kato, T.; López-Andarias, J.; Sakai, N.; Matile, S. Thiol-mediated uptake. *JACS Au* **2021**, *1* (6), 710−728.
(62) Wang, H.; Hu, Y.; Wang, Y.; Lu, J.; Lu, H. Doxorubicin@PEPylated interferon-polydisulfide: a multi-responsive nanoparticle for enhanced chemo-protein combination therapy. *Giant* **2021**, *5*, 100040−100047.
(63) Yuan, P.; Yang, F.; Liew, S. S.; Yan, J.; Dong, X.; Wang, J.; Du, S.; Mao, X.; Gao, L.; Yao, S. Q. Intracellular co-delivery of native antibody and siRNA for combination therapy by using biodegradable silica nanocapsules. *Biomaterials* **2022**, *281*, 121376−121388.
(64) Lu, J.; Wang, H.; Tian, Z.; Hou, Y.; Lu, H. Cryopolymerization of 1,2-Dithiolanes for the Facile and Reversible Grafting-from Synthesis of Protein-Polydisulfide Conjugates. *J. Am. Chem. Soc.* **2020**, *142* (3), 1217−1221.
(65) Wan, Y.; Wang, W.; Lai, Q.; Wu, M.; Feng, S. Advances in cell-penetrating poly(disulfide)s for intracellular delivery of therapeutics. *Drug Discovery Today* **2023**, *28* (8), 103668−103676.
(66) Trzciński, J. W.; Morillas-Becerril, L.; Scarpa, S.; Tannorella, M.; Muraca, F.; Rastrelli, F.; Castellani, C.; Fedrigo, M.; Angelini, A.; Tavano, R.; Papini, E.; Mancin, F. Poly(lipoic acid)-Based Nanoparticles as Self-Organized, Biocompatible, and Corona-Free Nanovectors. *Biomacromolecules* **2021**, *22* (2), 467−480.
(67) Liu, Y.; Jia, Y.; Wu, Q.; Moore, J. S. Architecture-controlled ring-opening polymerization for dynamic covalent poly(disulfide)s. *J. Am. Chem. Soc.* **2019**, *141* (43), 17075−17080.
(68) Brülisauer, L.; Gauthier, M. A.; Leroux, J.-C. Disulfide-containing parenteral delivery systems and their redox-biological fate. *J. Controlled Release* **2014**, *195*, 147−154.
(69) Gasparini, G.; Matile, S. Protein delivery with cell-penetrating poly(disulfide)s. *Chem. Commun.* **2015**, *51* (96), 17160−17162.
(70) Fu, J.; Yu, C.; Li, L.; Yao, S. Q. Intracellular delivery of functional proteins and native drugs by cell-penetrating poly(disulfide)s. *J. Am. Chem. Soc.* **2015**, *137* (37), 12153−12160.
(71) Yu, C.; Qian, L.; Ge, J.; Fu, J.; Yuan, P.; Yao, S. C.; Yao, S. Q. Cell-Penetrating Poly(disulfide) Assisted Intracellular Delivery of Mesoporous Silica Nanoparticles for Inhibition of miR-21 Function and Detection of Subsequent Therapeutic Effects. *Angew. Chem., Int. Ed.* **2016**, *55* (32), 9272−9276.
(72) Lu, J.; Xu, Z.; Fu, H.; Lin, Y.; Wang, H.; Lu, H. Room-Temperature Grafting from Synthesis of Protein−Polydisulfide Conjugates via Aggregation-Induced Polymerization. *J. Am. Chem. Soc.* **2022**, *144* (34), 15709−15717.
(73) Cheng, Y.; Pham, A.-T.; Kato, T.; Lim, B.; Moreau, D.; López-Andarias, J.; Zong, L.; Sakai, N.; Matile, S. Inhibitors of thiol-mediated uptake. *Chem. Sci.* **2021**, *12* (2), 626−631.
(74) Lim, B.; Cheng, Y.; Kato, T.; Pham, A. T.; Le Du, E.; Mishra, A. K.; Grinhagena, E.; Moreau, D.; Sakai, N.; Waser, J.; Matile, S. Inhibition of thiol-mediated uptake with irreversible covalent inhibitors. *Helv. Chim. Acta* **2021**, *104* (8), No. e2100085, DOI: 10.1002/hlca.202100085.
(75) Liu, K.; Zheng, L.; Liu, Q.; de Vries, J. W.; Gerasimov, J. Y.; Herrmann, A. Nucleic Acid Chemistry in the Organic Phase: From Functionalized Oligonucleotides to DNA Side Chain Polymers. *J. Am. Chem. Soc.* **2014**, *136* (40), 14255−14262.
(76) Brown, M. S.; Goldstein, J. L.; Receptor-Mediated, A. Pathway for Cholesterol Homeostasis. *Science* **1986**, *232* (4746), 34−47.
(77) Wilson, P. W. F.; D'Agostino, R. B.; Levy, D.; Belanger, A. M.; Silbershatz, H.; Kannel, W. B. Prediction of Coronary Heart Disease Using Risk Factor Categories. *Circulation* **1998**, *97* (18), 1837−1847.
(78) Gennemark, P.; Walter, K.; Clemmensen, N.; Rekić, D.; Nilsson, C. A. M.; Knöchel, J.; Hölttä, M.; Wernevik, L.; Rosengren, B.; Kakol-Palm, D.; Wang, Y.; Yu, R. Z.; Geary, R. S.; Riney, S. J.; Monia, B. P.; Isaksson, R.; Jansson-Löfmark, R.; Rocha, C. S. J.; Lindén, D.; Hurt-Camejo, E.; Crooke, R.; Tillman, L.; Rydén-Bergsten, T.; Carlsson, B.; Andersson, U.; Elebring, M.; Tivesten, A.; Davies, N. An oral antisense oligonucleotide for PCSK9 inhibition. *Sci. Transl. Med.* **2021**, *13* (593), No. eabe9117, DOI: 10.1126/scitranslmed.abe9117.
(79) Khvorova, A.; Watts, J. K. The chemical evolution of oligonucleotide therapies of clinical utility. *Nat. Biotechnol.* **2017**, *35* (3), 238−248.